Journal of Crystal Growth ▮ (▮▮▮▮) ▮▮▮–▮▮▮

Contents lists available at ScienceDirect

Journal of Crystal Growth

journal homepage: www.elsevier.com/locate/jcrysgro

TEM investigations on growth interrupted samples for the correlation of the dislocation propagation and growth mode variations in AlGaN deposited on SiN_x interlayers

O. Klein [a,*], J. Biskupek [a], K. Forghani [b], F. Scholz [b], U. Kaiser [a]

[a] Central Facility of Electron Microscopy, Group of Electron Microscopy for Materials Science, Ulm University, 89081 Ulm, Germany
[b] Institute of Optoelectronics, Ulm University, 89081 Ulm, Germany

ARTICLE INFO

Article history:
Received 29 November 2010
Received in revised form
9 March 2011
Accepted 29 March 2011
Communicated by T. Paskova

Keywords:
A1. Dislocations
A1. EDX
A1. Transmission electron microscopy
A3. Metalorganic vapour phase epitaxy
B2. AlGaN
B2. SiN

ABSTRACT

Threading dislocations (TDs) can be reduced by in-situ deposition of intermediate SiN_x sub-monolayers in group III-nitride heterostructures and their ternary alloys. Here we observe efficient dislocation density decreasing at the SiN_x nano-mask in an $Al_xGa_{1-x}N$ layer with $x=0.2$ grown epitaxially on c-plane sapphire by low pressure MOVPE. However we did not achieve high annihilation efficiency homogenously along the whole SiN_x interface in our samples. Areas with high and low annihilation grade alternate along the interface in accordance with respective variations in the SiN_x distribution. Furthermore an unusual dislocation bundling was observed for the dislocations in areas with high dislocation densities above the SiN_x interface, leading to large areas of several μm^2 with low dislocation densities at the surface between the dislocation bundles. By using growth interrupted samples under same growth conditions, it was possible to investigate the heterostructures in different growth stages by cross-sectional TEM. This enabled us to correlate the dislocation propagation with growth mode variations in AlGaN deposited on the SiN_x interlayer and to develop a growth model for the AlGaN layer grown on the SiN_x nano-mask.

1. Introduction

AlGaN with high Al concentration has attracted great attention because of its potential application to optoelectronic devices in the UV range due to its large direct band gap of up to 6 eV. In contrast to already commercially available blue and green light-emitting diodes (LEDs) with InGaN active layers, where localized energy states caused by In composition fluctuations are believed to improve the emission efficiency [1], the performance of deep UV LEDs based on AlGaN is much more sensitive to crystalline defects. In order to avoid UV light absorption by any GaN buffer layer, the ternary layer AlGaN should be grown directly on sapphire (Al_2O_3), as adequate nitride based substrates are not yet readily available. Hence, all hetero epitaxy problems like large lattice mismatch and difference in thermal expansion coefficients still exist, and the epitaxial growth of AlGaN as a ternary, Al containing material is even more challenging and less developed up to now than the growth of GaN [2–6]. Especially **a**-type threading dislocations (TDs) are responsible for still high dislocation densities in the $10^{10}\,cm^{-2}$ range, which can act as non-radiative recombination centres and thus lower the efficiency and the lifetime of the optoelectronic device [7–9]. One method to reduce the TD density in (Al,Ga)N layers is the use of epitaxial lateral overgrowth (ELO), which is widely used to grow high quality GaN layers [10,11] and has also been adapted to AlGaN [12]. However ELO is combined with typical drawbacks, such as complex ex-situ masking procedures and the presence of TDs in the window regions. Moreover it has been shown by Mochizuki et al. [13], that conventional ELO growth is not suitable for AlGaN. Another promising possibility to decrease the dislocation density of an AlGaN surface is the in-situ growth of intermediate SiN_x sub-monolayers [14–17]. Treating the AlGaN layers with SiH_4 and NH_3 in the MOVPE reactor leads to a fractional coverage of the surface of the layer with SiN_x. As SiN_x acts as an anti-surfactant the SiN_x nano-mask leads to a three-dimensional insular growth of the subsequently grown AlGaN with a lateral overgrowth of the SiN_x islands, which makes the TDs to change their propagation into a basal direction. The subsequent interaction of the upper ends of two TDs with Burgers vectors of opposite sign leads to the formation of closed dipoles close to the SiN_x mask and therefore to a reduction of the dislocation density [16]. Such annihilation process was described in Ref. [18] for **c**-type screw dislocations in pure GaN by silicon delta-doping (δSi). However they showed that the δSi does not affect the edge component of dislocations. In our

* Corresponding author.
E-mail address: oliver.klein@uni-ulm.de (O. Klein).

0022-0248/$ - see front matter © 2011 Elsevier B.V. All rights reserved.
doi:10.1016/j.jcrysgro.2011.03.050

previous work we could observe the formation of closed dipoles for the **a**-type TDs at the SiN_x nano-mask in an $Al_xGa_{1-x}N$ layer with $x=0.2$ grown directly on c-plane sapphire by low pressure MOVPE without the use of a UV absorbing GaN buffer layer. However the defect reducing effect of the SiN_x nano-mask is highly efficient only locally along the SiN_x interface. Areas with high and low annihilation grade alternate along the interface. Furthermore an unusual dislocation bundling was observed for the dislocations in areas with low annihilation grade above the SiN_x interface. The general change of the propagation direction of the not annihilated TDs away from the areas with high annihilation grade leads to large areas of several μm^2 at the surface with low dislocation densities between the bundles. This bundling effect as well as the not homogenous annihilation efficiency along the SiN_x interface are not well understood yet and give reason to further studies by TEM. The idea was to investigate samples under same growth conditions, where the growth was stopped after specific overgrowth times of the AlGaN layer, deposited above the SiN_x. Thus it was possible to investigate the AlGaN growth after SiN_x in different growth stages, which enabled us to correlate the changes in the dislocation propagation with variations in the AlGaN epitaxy. Cross-sectional weak-beam dark-field (WBDF), high-resolution (HR) TEM as well as energy dispersive X-ray (EDX) investigations on the growth interrupted samples led to the development of a growth model for the AlGaN epitaxy on the SiN_x nano-mask, which gives us a deeper insight into the growth mechanisms of AlGaN influenced by the SiN_x deposition.

2. Experimental methods

2.1. Growth parameters of investigated samples

We focused our studies on three different samples, denoted by S1, S2 and S3 in this work. All three samples were grown under the same growth conditions on c-plane sapphire (Al_2O_3) in the MOVPE reactor with the exception of different overgrowth times for the $Al_{0.2}Ga_{0.8}N$ layer, deposited on the SiN_x interface. They were grown by low pressure MOVPE at a temperature of 1120 °C and a pressure of 80 hPa, using trimethylaluminium/-gallium (TMAl/Ga) and ammonia (NH_3) as precursors. For all samples the growth was started by a low temperature 20-nm-thick oxygen doped AlN:O nucleation layer to improve the crystal quality [19], followed by a 150-nm-thick high temperature $Al_{0.2}Ga_{0.8}N$ layer. Subsequently an intermediate nominal SiN_x sub-monolayer was in-situ deposited on the $Al_{0.2}Ga_{0.8}N$, using silane (SiH_4) as precursor with a deposition time of 4 min at a pressure of 160 hPa and at the same temperature as for AlGaN growth [20,21]. The growth of sample S1 was completed by a 1-μm-thick $Al_{0.2}Ga_{0.8}N$ layer, whereas the growth of the same layer was stopped after 4 and 13 min for sample S2 and S3, respectively. Considering typical empirical growth rates of $\sim$1.3 μm h^{-1} for $Al_{0.2}Ga_{0.8}N$ we expected nominal thicknesses of $\sim$90 nm and $\sim$280 nm for the AlGaN overlayers in sample S2 and S3, respectively.

2.2. TEM investigations and imaging

For cross-sectional TEM investigations thin TEM lamellas were prepared by using standard techniques including mechanical polishing and low-angle argon milling [22]. The analysis of the TDs has been carried out by using the WBDF technique exploiting the $\mathbf{g}\cdot\mathbf{b}$ criterion, making use of the fact that $|\mathbf{g}\cdot\mathbf{b}|^2$ is proportional to the intensity of the dislocation line in the image [23]. The WBDF images were recorded under the **g**-3**g** condition close to the [01-10] zone axis. In wurtzite 2H AlGaN three different types of Burgers vectors **b** are possible for perfect dislocations. Referring to the $\mathbf{g}\cdot\mathbf{b}$ criterion, the **a**-type TDs with **b** of type 1/3 [2-1-10] and the (**a**+**c**)-type TDs with **b** of type 1/3 [2-1-13] are visible in the WBDF image when the 2-1-10 reflection is used. Exploiting the 0002 reflection, the (**a**+**c**)-type TDs as well as the **c**-type TDs with **b**=[0 0 0 1] are visible in the WBDF image, whereas the **a**-type TDs do not give rise to a contrast. Normally the growth induced TDs propagate parallel to the *c*-axis to the surface, if the AlGaN layer grows epitaxially in vertical direction on c-plane sapphire. Thus, the **a**-type TDs are pure edge and the **c**-type TDs are pure screw dislocations. The (**a**+**c**)-type TDs are of mixed type. Beside the WBDF method, HRTEM investigations were performed close to the SiN_x interface for detailed studies regarding the SiN_x deposition itself as well as the effects of the SiN_x nano-mask on the growth properties of the above AlGaN layer, such as the formation of dislocation loops and stacking faults. The WBDF investigations were carried out with a Philips CM-20 microscope, whereas the HRTEM images were taken in a FEI TITAN 80-300.

2.3. Analytical TEM by energy dispersive X-ray spectroscopy (EDX)

As mentioned above, the annihilation efficiency of the SiN_x interlayer changes along the interface. The reason for that was assumed to be variations in the Al/Ga content of the bottom AlGaN layer, influencing the SiN_x deposition. To clarify this, EDX measurements were performed by selective single measurements at the SiN_x interlayer, putting large astigmatism to the condenser system to obtain a sharp, straight-lined illumination of the specimen along the SiN_x interface. Additionally, locally resolved EDX measurements were carried out to measure changings in the Al/Ga concentration by performing EDX line-scans at low spot-sizes parallel to the SiN_x nano-mask below and above this interface. The EDX spectra were quantitatively evaluated by applying the ionic compound method of Van Cappellen and Doukhan, which has turned out to be suitable also for III–V semiconductors [24].

3. Results and discussion

3.1. Reduction of the threading dislocation density by a SiN_x nano-mask

Fig. 1 shows TEM images from the same specimen region of sample S1. The general layer structure is marked in the BF image in Fig. 1(a). The images were taken in an area of high annihilation grade for the TDs at the SiN_x interface. In addition we observe a homogenous dislocation density in the AlGaN layer below the SiN_x interface. The WBDF image in Fig. 1(b) under the 2-1-10 reflection only shows dislocations with Burgers vectors of type **a** and (**a**+**c**). Exploiting the 0002 reflection in Fig. 1(c), only **c** and (**a**+**c**)-type dislocations are visible. Thus, most of the growth induced TDs below the SiN_x interface are pure edge **a**-type TDs, mainly responsible for the high dislocation densities in 10^{10} cm^{-2} range. The in-situ deposition of a SiN_x sub-monolayer leads to a very efficient reduction of the **a**-type TDs at the SiN_x interface, clearly visible in the BF and WBDF image (Fig. 1(a) and (b)).

As silicon acts as an anti-surfactant [15], a fractional coverage of the bottom AlGaN layer by SiN_x leads to a three-dimensional insular growth of the AlGaN overlayer in areas without SiN_x deposition. The subsequent lateral overgrowth of the SiN_x nano-islands by AlGaN changes the propagation of the TDs from the [0 0 0 1] direction into a basal one and the interaction of the upper ends of two TDs with Burgers vectors of opposite sign leads to the formation of closed dislocation dipoles directly above the

Please cite this article as: O. Klein, et al., J. Crystal Growth (2011), doi:10.1016/j.jcrysgro.2011.03.050

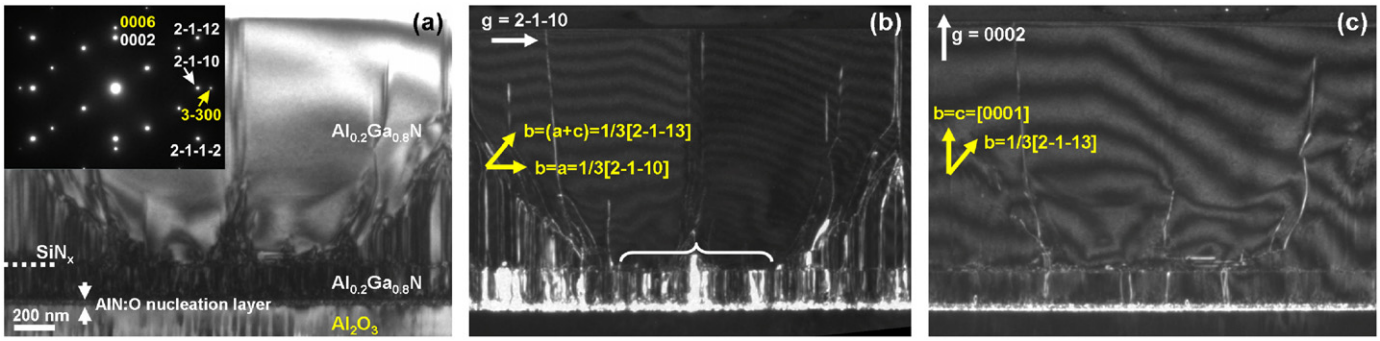

Fig. 1. Cross-section TEM images of sample S1. The BF image (a) from the [01-10] zone axis shows the AlGaN heterostructure on c-plane sapphire. The BF image as well as the WBDF images (b) and (c) were taken from the same sample area. The yellow arrows in (b) and (c) mark the Burgers vectors of the TDs visible for the respective g reflection. Regions of the SiN_x layer at which the annihilation of the pure edge a-type TDs is highly efficient are clearly observable (white marking in (b)). (For interpretation of the references to colour in this figure legend, the reader is referred to the web version of this article.)

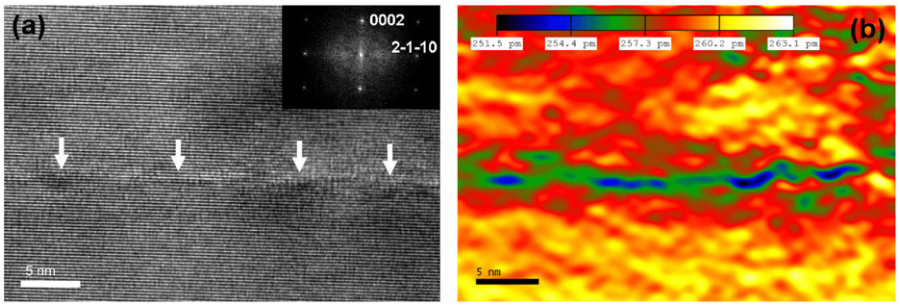

Fig. 2. The HRTEM image (a) and the respective geometric phase analysis for the (0002) reflection (b) clearly show the fractional coverage of AlGaN with SiN_x (white arrows in (a)). Besides, the SiN_x nano-mask introduces compressive strain into the material system in the [0001] direction. (For interpretation of the references to colour in this figure, the reader is referred to the web version of this article.)

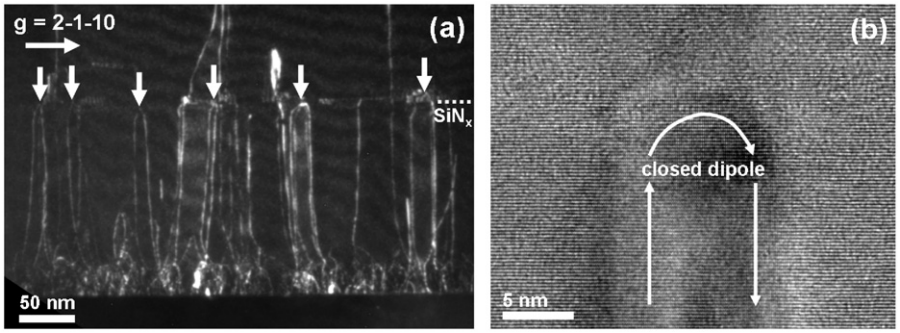

Fig. 3. The WBDF image (a) and the HRTEM image (b) show the a-type TDs in the area of the SiN_x interface at a zone of high annihilation grade. The formation of closed dislocation dipoles to dislocation half-loops is clearly visible (white arrows in (a)).

SiN_x mask. The HRTEM image in Fig. 2(a) from the [01-10] zone and the respective geometric phase analysis (GPA) in Fig. 2(b) of the 0002 reflection illustrates the fractional structure of the SiN_x nano-mask (blue regions in Fig. 2(b)). The GPA was performed in compliance with the explanations given in Ref. [25]. The false colour map shows the local d-spacing of the 0002 reflection and also indicates a compressive strain in [0 0 0 1] direction close to the SiN_x nano-mask. The formation of closed dislocation dipoles as the main reason for the dislocation reduction at the AlGaN surface is shown in Fig. 3. The 2-1-10 WBDF image (Fig. 3(a)) and the HRTEM image (Fig. 3(b)) clearly show the annihilation of the pure edge a-type threading dislocations by the formation of dislocation half-loops at the SiN_x interface. The interaction takes place between dislocations with a distance of only a few nanometres, which correlates with the distances and sizes of the SiN_x nano-islands. Detailed investigations and explanations on this annihilation process of the pure edge **a**-type TDs at a SiN_x interface itself have been carried out in our previous studies [16]. Here, the fractional coverage of the SiN_x and its distribution seems to be of major importance to obtain high annihilation efficiency. As it is known that dislocations can end at epitaxial interfaces [26], it would be conceivable that the propagation of the TDs is stopped at the SiN_x interlayer when regarding such layer as an epitaxial interface. Such termination was not observed in our samples. Instead, the lateral overgrowth of the SiN_x nano-mask by AlGaN and the associated formation of closed dislocation dipoles are essential for the defect reduction, which is in general accordance with the growth studies for pure GaN published in Ref. [27]. However they ascribed the formation of the half-loops to the coalescence of primary GaN islands in the overlayer. In our samples the formation of closed dipoles cannot be directly attributed to the coalescence of primary AlGaN islands in the

Please cite this article as: O. Klein, et al., J. Crystal Growth (2011), doi:10.1016/j.jcrysgro.2011.03.050

overlayer, as these islands can have a distance of several micrometres and the formation of dislocation half-loops takes place between dislocations with a distance of only a few nanometres as mentioned above. We will revisit this in more detail in this work, when we come to the question why we obtain different annihilation efficiencies along the SiN_x interface. The WBDF image in Fig. 4 shows an overview of the dislocation structure in sample S1. The areas with high annihilation grade at the SiN_x interface, already shown in Figs. 1 and 3, are clearly visible, whereas the dislocations propagate unhampered through the SiN_x interface between these areas (inset of Fig. 4). Most remarkable is the unusual but characteristic bending and bundling of the dislocations in areas with still high dislocation densities above the SiN_x interface. Regions of high annihilation efficiency in combination with the bundling effect lead to areas at the surface of several μm^2 with low defect densities between the bundles.

3.2. On the origin of the dislocation bundling—development of an AlGaN growth model

As described in the previous chapter, we observed a very characteristic dislocation structure for the growth of $Al_{0.2}Ga_{0.8}N$ on a SiN_x nano-mask. Regarding these investigations, it was necessary to clarify the reasons for the dislocation bundling and the variations in the annihilation efficiency, to achieve further progress in the reduction of the defect density in AlGaN layers with high Al content. Two basic driving forces can be considered for the bending and bundling of the dislocations: First, a strain induced propagation changing of the dislocations during the epitaxial growth of the AlGaN overlayer and second, variations of the epitaxial growth directions of the AlGaN, deposited on the SiN_x nano-mask. The latter only hardly can be retraced by a finished grown 1-μm-thick AlGaN overlayer with a flat surface like in sample S1. Thus, we carried out cross-sectional TEM investigations on growth interrupted samples for the AlGaN overlayer, grown under the same growth conditions as sample S1. This enabled us to investigate the AlGaN growth in different growth stages. We used two samples S2 and S3, where the growth of the AlGaN overlayer on SiN_x was stopped after 4 and 13 min, respectively. Fig. 5 shows SEM images of the AlGaN surface after 4 (Fig. 5(a)) and 13 min (Fig. 5(b)) overgrowth time. The SEM micrographs illustrate the growth of primary hexagonal-shaped AlGaN islands, increasing in lateral dimension. The coalescence of adjacent AlGaN islands after 13 min of overgrowth is clearly observable. Regarding the investigations on pure GaN published in Ref. [28], one could assume, that these islands are located at the SiN_x gaps, so that the SiN_x layer between the islands in Fig. 5 is free from AlGaN. However, Fig. 6 shows a different situation. The WBDF image in Fig. 6(a) of sample S2 as well as the BF images in Fig. 6(b) and (c) of sample S3 clearly illustrate the growth of primary AlGaN islands, marked by dashed lines. But in the flat regions between the AlGaN islands we observe an 80-nm-thick AlGaN layer already after 4 min of overgrowth time. These regions show high defect densities at the surface with straight dislocation lines due to a low annihilation efficiency of the subjacent SiN_x mask, also visible in the 230-nm-thick flat regions in Fig. 6(c) after an overgrowth time of 13 min. By contrast, the AlGaN islands are almost free of defects due to a high annihilation efficiency of the SiN_x mask below the islands. The initiating bending of the dislocations away from the islands and the resulting dislocation bundling as mentioned in Section 3.1 are already observable in sample S2 and S3. The change between the growth of flat AlGaN regions and exposed AlGaN islands in combination with their respective variations in the dislocation propagation indicate different growth modes with epitaxial growth directions in vertical as well as in lateral directions. As the growth of the AlGaN islands and the flat regions correlate with different annihilation grades, we assume, that variations in the SiN_x masking, resulting in different annihilation efficiencies, are responsible for different growth modes of the AlGaN overlayer. Fig. 6 also shows some special regions marked by rectangles, numbered by 1, 2 and 3. We will revisit these regions in detail in the further discussion.

A more detailed view on the dislocation structure is given by the WBDF images of sample S3 in Fig. 7. The image in Fig. 7(a) shows an area between two primary not yet coalesced AlGaN islands. The dashed arrows specify the general direction of the propagation of the TDs, not annihilated by the SiN_x mask. Between the islands the dislocations propagate unhampered parallel to the *c*-axis, whereas the bending of the dislocations

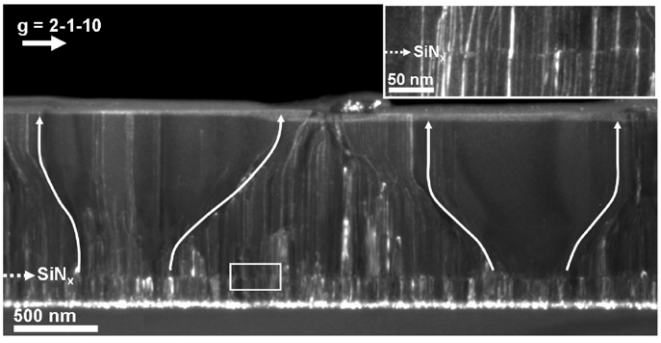

Fig. 4. Low magnification WBDF image exploiting the (2-1-10) reflection. The image shows a very unusual but characteristic bending and bundling of the a-type TDs, observed in the whole sample. The bundling (continuous arrows) always points away from the areas with high annihilation grade, leading to large areas of several μm^2 with low defect densities at the surface between the bundles. The inset of Fig. 4 shows an unhampered propagation of the dislocations through the SiN_x interface.

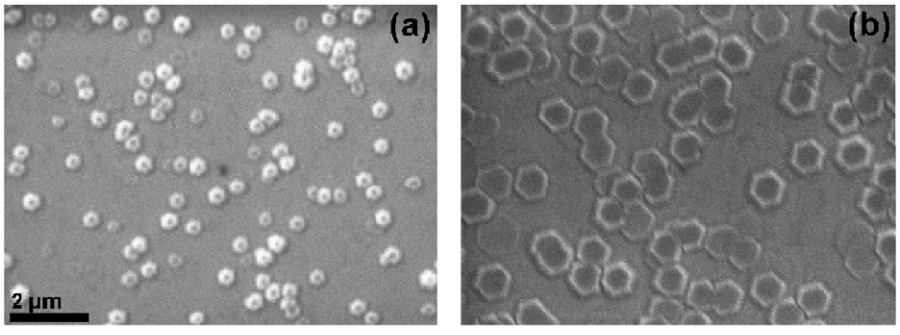

Fig. 5. SEM images of the surface of sample S2 (a) and S3 (b) after a growth time of 4 and 13 min of the AlGaN overlayer. The growth of primary hexagonal AlGaN islands is clearly visible, increasing in lateral size.

Please cite this article as: O. Klein, et al., J. Crystal Growth (2011), doi:10.1016/j.jcrysgro.2011.03.050

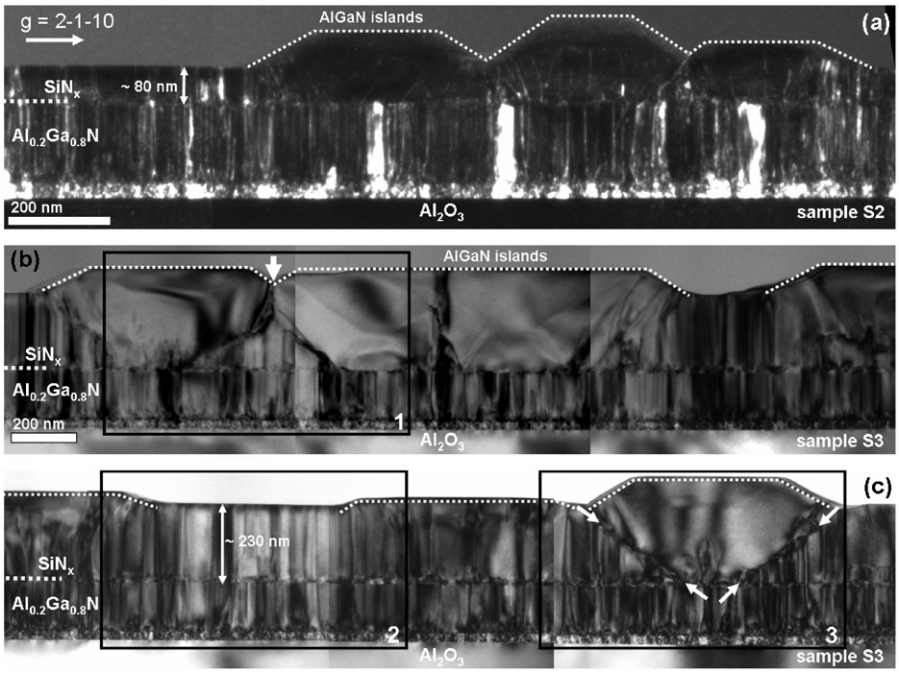

Fig. 6. Cross-sectional overview images of sample S2 (a) and S3 (b, c). The WBDF image (a) as well as the BF images (b, c) clearly show the growth of the primary AlGaN islands (dashed lines). The flat regions between the islands are not free of AlGaN (80 nm and 230 nm thickness). The low defect density and high annihilation grade always below the AlGaN islands is notable, whereas high defect densities and low annihilation grade is observed in the flat regions.

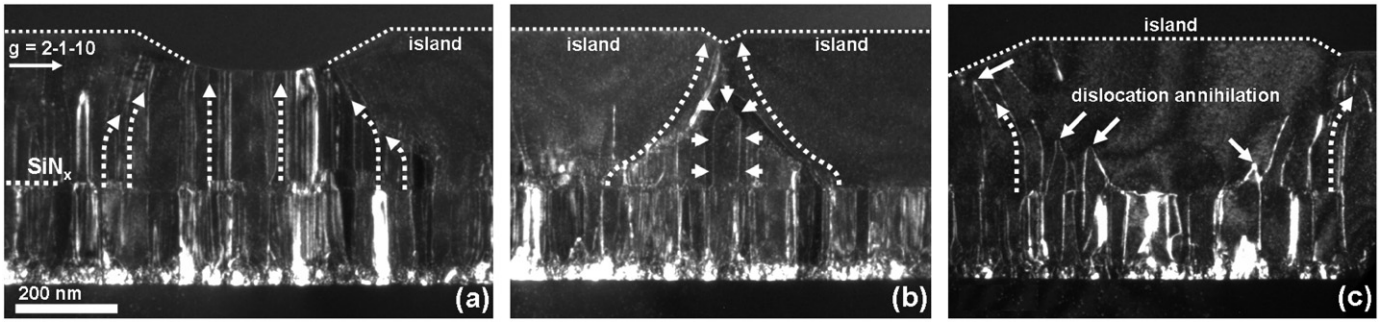

Fig. 7. WBDF images of sample S3 between two AlGaN islands (a, b) and in the centre of one island (dashed lines). The dashed arrows indicate the general propagation direction of the TDs in the AlGaN overlayer. Between not coalesced islands (a) the TDs run straight and the bending of the TDs away from areas with high annihilation grade is visible in all three images. The coalescence of two islands (b) leads to very small areas with TDs at the surface due to the bundling and the formation of dislocation loops (white arrows in b). The annihilation of the dislocations due to the bending effect is also possible (white arrows in (c)).

close to the defect-free areas away from the islands is evident. Thus, between the islands in areas with flat surface the deposition of the AlGaN overlayer occurs epitaxially in vertical *c*-direction. The growth of the AlGaN islands introduces an epitaxial growth component in lateral direction, leading to the dislocation bending and bundling. This leads to very small areas with high dislocation density at the surface, if two or more nearby AlGaN islands coalesce during growth, clearly visible in Fig. 7(b). Apart from the dislocation bundling, the lateral coalescence of the AlGaN islands has a defect reducing effect due to the formation of dislocation half-loops (white arrows in Fig. 7(b)). Also the bending itself leads to an interaction and annihilation of the dislocations at the interface between lateral and vertical growth (white arrows in Fig. 7(c)). Referring to Fig. 4, we receive a flat surface over the whole specimen after the growth of a 1-μm-thick AlGaN overlayer, regardless of an occurring or not occurring coalescence. This was additionally confirmed by AFM measurements also for larger overgrowth thicknesses, published in Ref. [29]. If two islands do not coalesce due to their large distance, relatively large areas in μm range with high dislocation densities at the surface develop due to less tight dislocation bundling. However, this also means, that the epitaxial growth in *c*-direction between the islands reaches the same level as the primary AlGaN islands after a specific growth thickness. When a flat surface is reached for the whole layer, the growth continues with a pure epitaxial growth in *c*-direction without lateral component. The bundled dislocations will then further propagate parallel to the *c*-axis. This is exactly the situation we have in Fig. 4.

So far we obtained a very detailed understanding about the growth process of the AlGaN overlayer, deposited on a SiN_x nanomask. To get a comprehensive understanding of the growth mechanisms and to develop a complete growth model, it has to be clarified, why the nucleation of the primary AlGaN islands is always located in areas with high annihilation grade and what is the possible reason for different annihilation efficiencies. The EDX measurements in Fig. 8, taken with same collection times of 60 s directly at the SiN_x interface, lead to an explanation for the different annihilation grades. A spread illumination of the sample

Please cite this article as: O. Klein, et al., J. Crystal Growth (2011), doi:10.1016/j.jcrysgro.2011.03.050

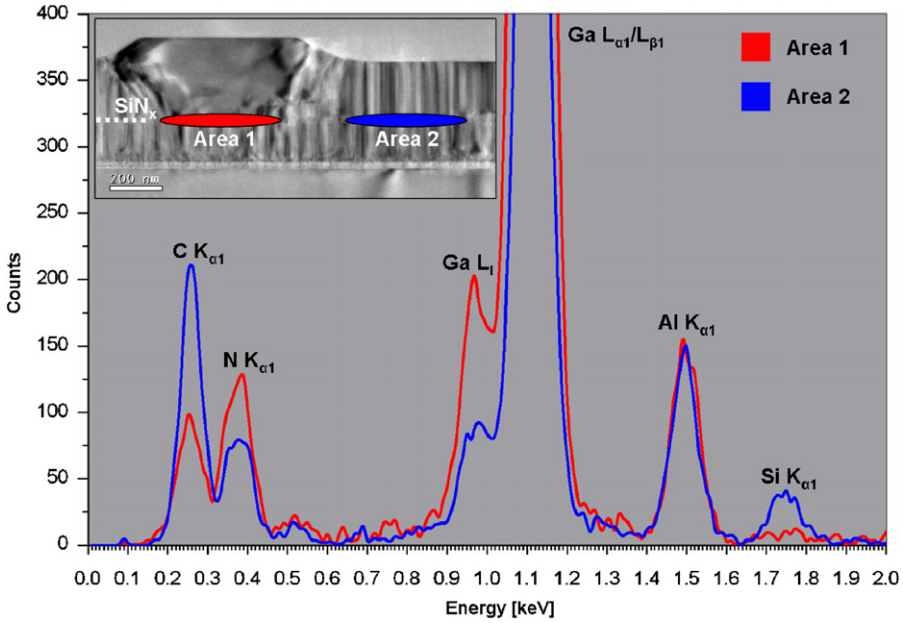

Fig. 8. EDX spectra taken with same collection times from two different areas at the SiN_x interlayer by using a spread illumination parallel to the interface to obtain a Si signal despite low concentrations. The EDX spectrum of area 2 shows a clear Si peak, whereas the Si is almost not measurable in area 1. It is remarkable, that Si is almost not detectable in areas with high annihilation grade. In addition variations in the Ga and N concentration are also observed.

parallel to the SiN_x interface was used, to get the chance for the detection of silicon despite the low silicon concentration in a nominal SiN_x monolayer. Silicon is almost not detectable in areas with high annihilation grade, whereas a clear silicon signal in areas with low annihilation efficiency was received. This is at first a very unexpected result, as one could think, that the defect reducing effect of the SiN_x interlayer should be enhanced in regions with higher silicon concentrations. However, the interpretation of this is quite obvious. In areas with high annihilation grade the bottom AlGaN layer is only fractionally covered with SiN_x nano-islands, which leads to the formation of the dislocation half-loops by lateral overgrowth and an almost not measurable silicon concentration. In areas with a closed SiN_x coverage and thus a measurable silicon concentration by EDX the closed dislocation dipoles cannot be generated due to the missing lateral overgrowth. In these areas the AlGaN overlayer is deposited epitaxially in *c*-direction and the dislocations further propagate unhampered through the SiN_x layer parallel to the *c*-axis (see inset of Fig. 4). Thus, a closed coverage with SiN_x does not preclude the AlGaN from nucleating on the anti-surfactant. This is in very good accordance to the investigations regarding the annihilation process of the dislocations at the SiN_x nano-mask, mentioned in Section 3.1. The fact that the AlGaN also grows on areas with a closed SiN_x coverage is consistent with the investigations published in [30] where the AlGaN is described to be less selective in growth than GaN. As the nucleation of the AlGaN overlayer is more favourable in regions between large SiN_x islands where the subjacent AlGaN layer is only fractionally covered by SiN_x nano-islands, a prior deposition of AlGaN with a balanced ratio of the epitaxial vertical and lateral growth component occurs after the lateral overgrowth of the SiN_x nano-islands is completed. This is the origin for the formation of the primary AlGaN islands. The vertical growth component in the central region of a primary AlGaN island is indicated by TDs not annihilated at the SiN_x mask in regions of high defect reducing efficiency, propagating to the surface without bending (visible between the two left bundling marks in Fig. 4). To get on one step further regarding the defect reduction, it is essential to clarify the reason for the varying SiN_x distribution, leading to different annihilation efficiencies. In addition to our first EDX measurements in Fig. 8, locally resolved EDX data were acquired along two manually operated scan-lines below and above the SiN_x layer parallel to the interface to measure the Al, Ga and N concentration in an area of an AlGaN island (Fig. 9). The local resolution was in the range of 70 nm, given by the illuminating beam diameter. The quantitative evaluation of the spectra clearly shows an increasing substitution of Al by Ga below the SiN_x interface in the area where the AlGaN island is located. The nominal Al, Ga and N concentrations in $Al_{0.2}Ga_{0.8}N$ of 10, 40 and 50 at%, respectively, change to concentrations of 5 at% for Al and 45 at% for Ga, whereas the Al, Ga and N concentrations stay stable in the range of their nominal values above the SiN_x interface. In the regions to the left and right of the AlGaN island the Al and Ga concentrations below the SiN_x interface also deviate slightly ($\sim$2 at%) from the concentrations measured above SiN_x. These correlations were confirmed by additional EDX line-scans similar to Fig. 9 at three different AlGaN islands, always showing the same behaviour of the concentration variations. Similar local compositional variations of AlGaN epitaxial films measured by EDX have been reported in Ref. [6]. In their work concentration fluctuations during AlGaN growth were ascribed to morphological irregularities of the nucleation layer and occur during the initial growth stage. Additional CL and PL measurements on such AlGaN islands, published in Ref. [31], showed, that the amount of Al and Ga incorporated during growth can depend on the orientation of the growth facets. Unfortunately it is hard to say, if the changing of the Al/Ga concentration is directly responsible for the variation of the SiN_x distribution and thus for the annihilation efficiency of the SiN_x mask. However, the correlation between the variations in the Al/Ga concentration and the areas with high annihilation grade and the corresponding position of the AlGaN islands is obvious. It could be inferred from the measurement of an increased Ga concentration in the AlGaN layer below areas of high annihilation efficiency, that the Ga/Al terminated layer directly beneath SiN_x also has an increased Ga concentration, directly influencing the SiN_x deposition and distribution.

Based on our measurements, Figs. 10 and 11 illustrate schematically the whole growth process of the AlGaN overlayer on the SiN_x

Please cite this article as: O. Klein, et al., J. Crystal Growth (2011), doi:10.1016/j.jcrysgro.2011.03.050

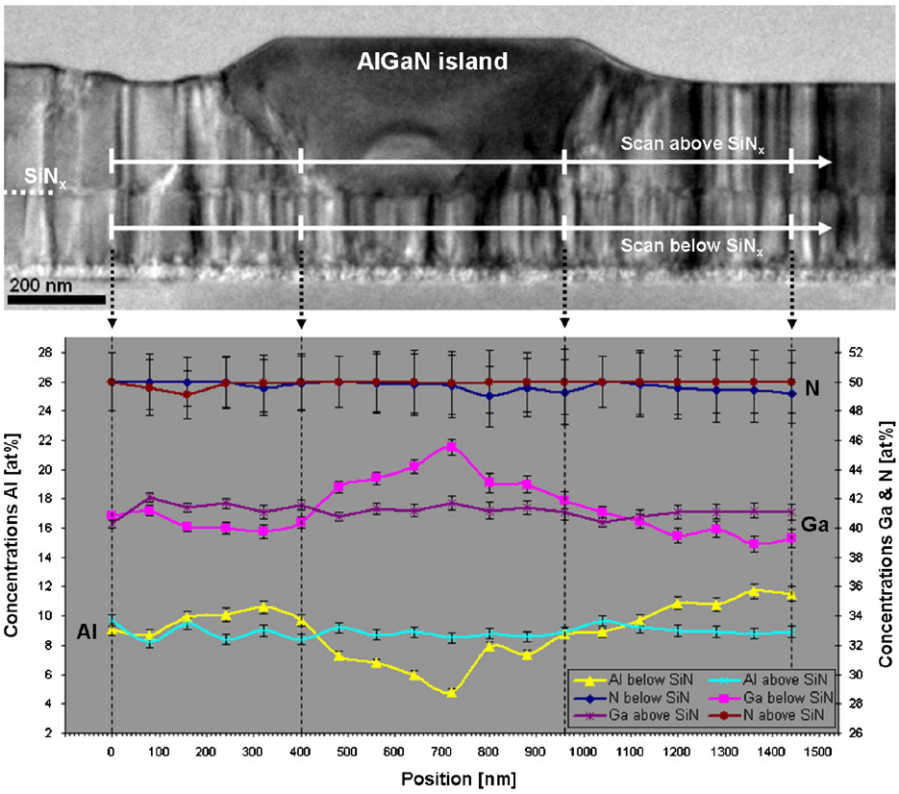

Fig. 9. Measurement of the Al, Ga and N concentrations along a primary AlGaN island directly above and below the SiN_x interface by performing locally resolved EDX line-scans. An increasing Ga and decreasing Al concentration can be observed in regions below the AlGaN island, whereas the Al, Ga and N concentrations stay stable in the range of their nominal values of 10, 40 and 50 at% above the interface, respectively.

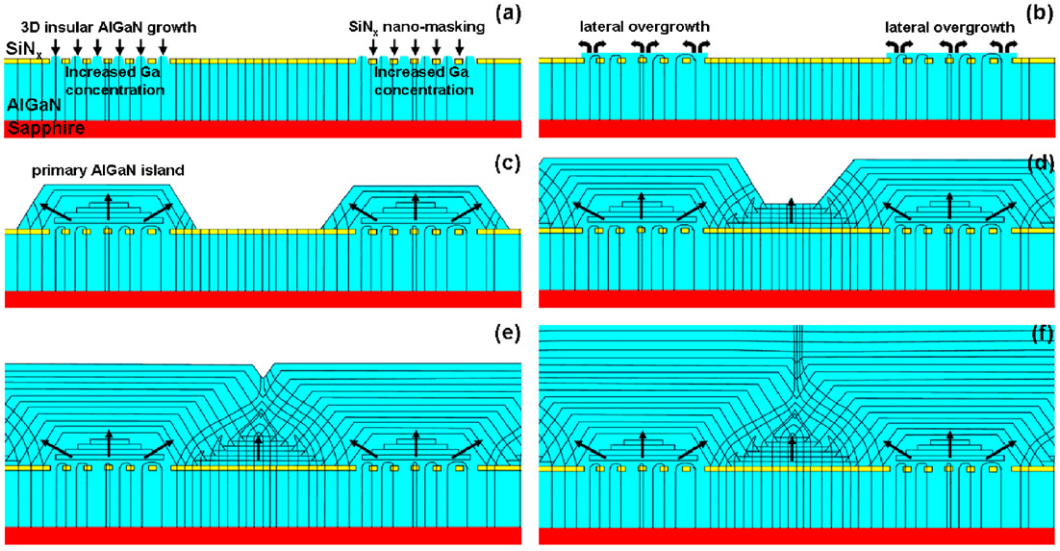

Fig. 10. Growth model for the coalescence of two nearby primary AlGaN islands, illustrated in consecutive growth steps (a–f). The nucleation of the islands is located in areas with high annihilation efficiency, i.e. in areas where the AlGaN is only fractionally covered with SiN_x nano-islands. The arrows in (b) indicate the lateral overgrowth of the SiN_x nano-mask, responsible for the formation of the dislocation half-loops. The arrows in the images (c)–(f) show the epitaxial vertical and lateral growth directions. The latter leads to the dislocation bending and bundling. The coalescence results in only very small areas at the surface with high dislocation densities (f).

nano-mask with a different distribution of the SiN_x nano-islands. As mentioned above, two growth mechanisms can be distinguished, depending on the distance of two primary AlGaN islands. Fig. 10 shows the growth and coalescence of two nearby islands, leading to small areas with high defect densities at the surface. The situation in Fig. 10(d) is exactly what can be observed in the TEM images (Fig. 6(a) and Fig. 7(a) and (c)). The almost finished coalescence in Fig. 10(e) is visible in the highlighted area 1 in Figs. 6(b) and 7(b). If two AlGaN islands are widely spaced like in Fig. 11, the epitaxial growth in *c*-direction between the AlGaN islands will reach the level of the islands before they can coalesce. This leads to larger areas with high defect densities at the surface. The growth stage in Fig. 11(c) and (d) is exactly what we obtained in TEM in the highlighted area 2 in Figs. 6(c) and 4, respectively.

Please cite this article as: O. Klein, et al., J. Crystal Growth (2011), doi:10.1016/j.jcrysgro.2011.03.050

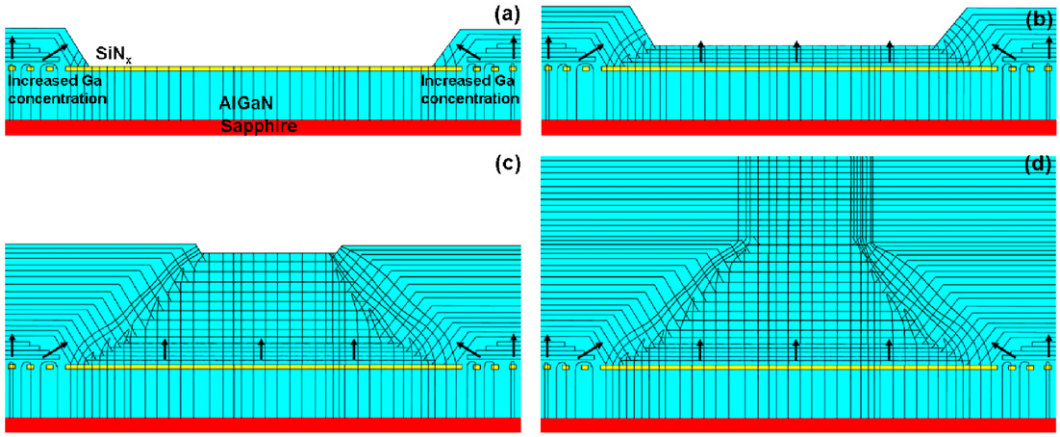

Fig. 11. Growth model in case of two fairly distant AlGaN islands, illustrated in consecutive growth steps (a–d). In contrast to Fig. 10, the not occurring coalescence leads to large areas at the surface with high dislocation densities (d).

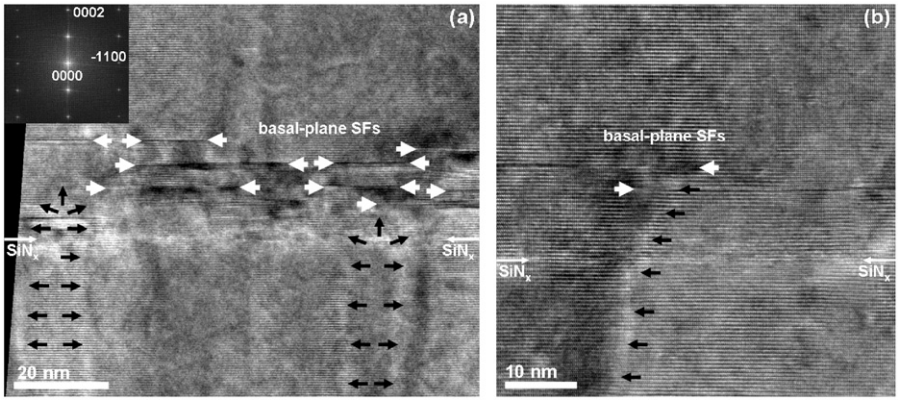

Fig. 12. HRTEM images of sample S1 from the [11–20] zone in the range of the SiN_x interface. The images show the formation of basal-plane stacking faults directly above the SiN_x mask. The black arrows mark the propagation of the TDs. Image (a) clearly shows the formation of dislocation half-loops as mentioned in Section 3.1. In contrast, image (b) illustrates the formation of BSFs by dissociation of a single TD, not further propagating to the surface.

3.3. *Formation of stacking faults in accordance to the growth mode variations*

As mentioned already in Section 3.1, a fractional coverage with an optimum distribution of SiN_x is essential for high annihilation efficiencies, enabling the dislocations to form half-loops by lateral AlGaN overgrowth. In addition another defect reducing effect has to be considered precluding the TDs from propagating further to the surface. We could observe the formation of basal-plane stacking faults (BSFs) in areas correlating with specific regions in our growth model. The HRTEM image from the [11-20] zone in Fig. 12(a) shows an accumulation of BSFs directly above the SiN_x interface in a region of high defect reduction, whereas the AlGaN overlayer is free of BSFs in regions more than 30 nm away from the SiN_x interface. This suggests, that the formation of the BSFs is related to the SiN_x nano-mask, introducing lateral growth directions into the AlGaN overlayer. The lateral overgrowth of SiN_x by AlGaN and the subsequent coalescence of the AlGaN nano-islands can lead to the formation of BSFs. The formation of several dislocation half-loops as we know already from our previous investigations is also visible in Fig. 12(a). In contrast, Fig. 12(b) shows a single dislocation which does not further propagate to the surface where the BSF is located. In general it is known, that vertical dislocations can disappear at BSFs, formed in low temperature pure GaN buffer layers [32]. Here we assume, that these stacking faults can be formed directly after dissociation of a perfect dislocation with **b** of type 1/3 [2–1–10] in two Shockley partials, as this process is known as the most likely case for the formation of BSFs in connection with perfect dislocations in GaN [14]. The stacking fault is then terminated by two Shockley partial dislocations with Burgers vectors $\mathbf{b}=1/3$ [1–100] and 1/3[10–10], which can glide on the {0001} slip plane. Fig. 13 shows the HRTEM analysis of a single BSF close above the SiN_x interface. The magnified area in Fig. 13(b) definitely identifies the planar defect as a BSF with a single violation in the stacking sequence, i.e. ABABABCBCBCBC. Such intrinsic I_1 type stacking fault has to be bounded by a Frank–Shockley partial dislocation with Burgers vector $\mathbf{b}=1/6$ [20–23]. It is known, that the I_1 type BSF is likely to be formed during the growth process and not due to distortions induced by stress during or after growth [33]. This confirms the assumption, that the BSFs are formed during the growth process due to the lateral coalescence of the AlGaN nano-islands, induced by the overgrowth of the SiN_x anti-surfactant by AlGaN.

Also remarkable is a special arrangement of most BSFs in a direction correlating with the interface of interacting vertical and lateral growth directions in our growth model. Fig. 14 shows this relationship. BSFs with a stacked arrangement along the boundary of the dislocation bundling can be observed, reaching deep into the AlGaN overlayer away from the SiN_x interface. The investigated region is marked in Fig. 14(a) and correlates with regions where vertical and lateral growth directions of the AlGaN overlayer coincide alternately. The respective region in our growth model is given in Fig. 14(b) and the placement of the experimentally observed BSFs is also illustrated in the model. The HRTEM image in Fig. 14(c) clearly shows some TDs not further propagating to the surface at BSFs similar to the process described above. The formation of these BSFs by dissociation of perfect

Please cite this article as: O. Klein, et al., J. Crystal Growth (2011), doi:10.1016/j.jcrysgro.2011.03.050

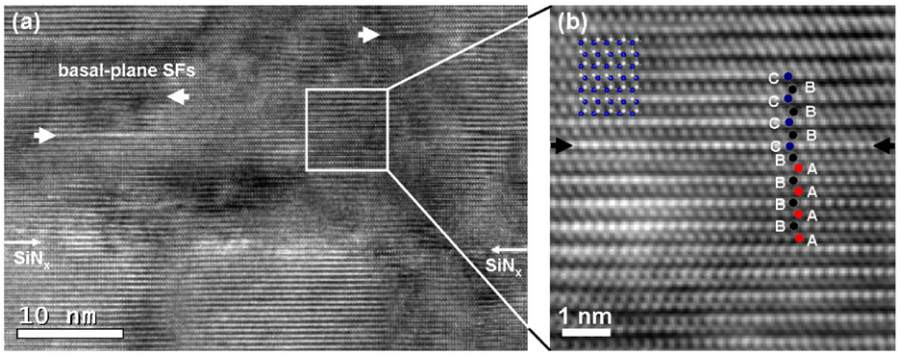

Fig. 13. HRTEM analysis of a single basal-plane stacking fault. The magnified area in image (b) identifies the planar defect as a single violation in the stacking sequence, i.e. ABABABCBCBC.

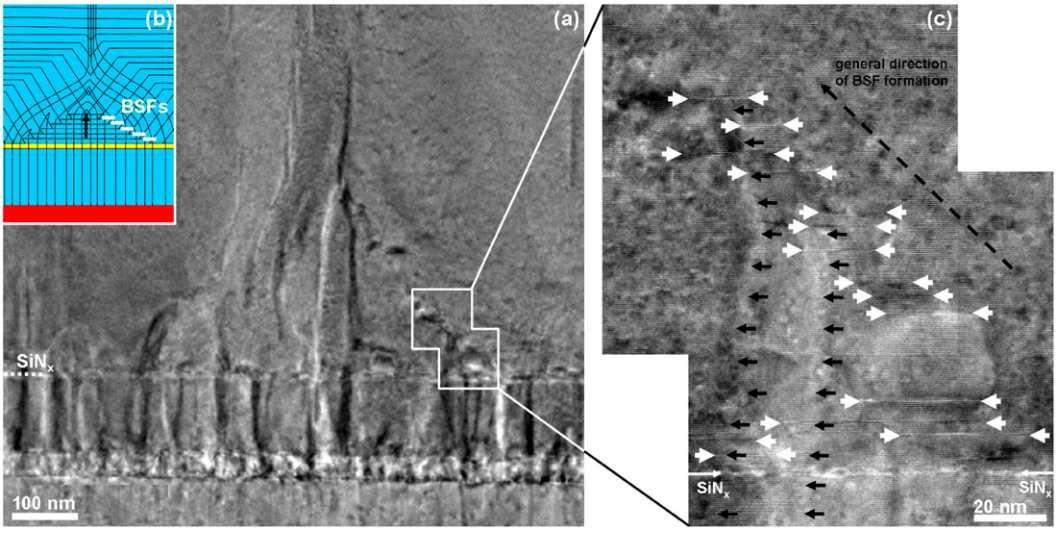

Fig. 14. Formation of basal-plane stacking faults (white arrows in c) with increasing distance to the SiN_x interface. Regarding our growth model (b), the special arrangement of the stacking-faults correlates with the interface of interacting vertical and lateral growth directions. The disappearance of the TDs (black arrows in c) at BSFs is clearly visible.

dislocations can be the reason for the occurrence of relatively sharp boundaries between high and low defect regions in some primary AlGaN islands. As an example, such region is given in the highlighted area 3 in Fig. 6(c). The white arrows mark the line where the BSFs are generated and the TDs disappear. We conclude that growth induced BSFs and BSFs formed by dissociation of TDs occur in regions, which are associated with growth mode variations in accordance with the growth model. Thus the origin of these BSFs may be assigned to local irregularities in AlGaN epitaxy, as these BSFs occur in regions where different epitaxial growth directions interact with reference to the growth model. The lateral growth component of AlGaN can change the propagation of a TD into a basal direction. It is known that the dislocation lying in the {0001} basal plane is easily dissociated due to the low energy of the stacking fault in the basal plane [34,35]. In addition, the dissociation of the TDs can reduce the dislocation density as they do not further propagate to the surface.

4. Summary and conclusions

In this work we presented a growth model for the growth of an $Al_{0.2}Ga_{0.8}N$ overlayer on a SiN_x nano-mask. This was possible by a phenomenological approach on the basis of cross-sectional TEM studies on growth interrupted samples. We found that the dislocation bending and bundling have to be ascribed to growth mode variations of the AlGaN overlayer, depending on the SiN_x coverage and distribution. The growth of primary AlGaN islands with a vertical and lateral growth component in areas with high annihilation grade alternates with the growth of a flat AlGaN layer with only a growth component in *c*-direction in areas with low annihilation efficiency. The EDX measurements showed a high Si concentration at the SiN_x interface in regions where the TDs propagate unhampered through the interlayer to the surface, whereas Si was almost not measurable at the SiN_x interface in regions with high annihilation grade. Thus, to achieve a high defect reducing effect of the SiN_x nano-mask a fractional coverage of SiN_x with a distribution of the SiN_x nano-islands in nanometre range is essential for the formation of closed dislocation dipoles by lateral overgrowth. This means that the formation of the dislocation half-loops cannot be ascribed directly to the lateral coalescence of the primary AlGaN islands, which can have distances of several micrometres. In fact the formation of dislocation half-loops as the main defect reducing process is attributed to the overgrowth of nanometre-sized SiN_x islands within one primary AlGaN island. A closed coverage with SiN_x induces no lateral overgrowth and thus no defect reducing effect. However, a second effect for the defect reduction has to be considered beside the annihilation by the formation of dislocation half-loops.

Please cite this article as: O. Klein, et al., J. Crystal Growth (2011), doi:10.1016/j.jcrysgro.2011.03.050

The formation of BSFs by dissociation of TDs into partial dislocations precludes the TDs from further propagating to the surface. It is remarkable, that growth induced BSFs and BSFs formed by dissociation of TDs are observed in regions of the AlGaN overlayer, which can be related to growth mode variations in accordance with the growth model. We conclude that the key for a uniformly low defect density at the surface of a MOVPE grown $Al_{0.2}Ga_{0.8}N$ layer is the optimum distribution of SiN_x by nanometre-sized SiN_x islands over the whole template. Unfortunately the SiN_x deposition and distribution can only be engineered indirectly by the growth temperature and the SiH_4 inlet time. However, our locally resolved EDX measurements also show a connection between variations in the Al/Ga concentration below the SiN_x interface and the SiN_x coverage. The WBDF analyses and the high-resolution GPA measurements in connection with the concentration measurements by EDX show, that an optimum distribution of SiN_x is obtained in regions where Al is increasingly substituted by Ga with compositional variations in the range of up to 5 at% in the previously grown $Al_{0.2}Ga_{0.8}N$ buffer layer. Thus the changing SiN_x coverage, leading to growth mode variations in the AlGaN overlayer, might be the consequence of variations in the Al/Ga concentration. Therefore, compositional variations in the AlGaN buffer layer seem also to be a decisive parameter for the optimization of the SiN_x distribution.

Acknowledgements

We are grateful to Dr. Igor Khodos for stimulating discussions on growth induced dislocation mechanisms. We would like to thank S. Grözinger for sample preparation. This work was financially supported by the Bundesministerium für Bildung und Forschung (BMBF) in the framework of the "Deep UV-LED" project.

References

[1] T. Mukai, D. Morita, S. Nakamura, U.V. High-power, InGaN/AlGaN double-heterostructure LEDs, J. Cryst. Growth 189/190 (1998) 778–781.
[2] N. Kuwano, T. Tsuruda, Y. Kida, H. Miyake, K. Hiramatsu, T. Shibata, TEM analysis of threading dislocations in crack-free $Al_xGa_{1-x}N$ grown on an AlN(0001) template, Phys. Status Solidi C 0 (7) (2003) 2444–2447.
[3] S.B. Thapa, C. Kirchner, F. Scholz, G.M. Prinz, K. Thonke, R. Sauer, A. Chuvilin, J. Biskupek, U. Kaiser, D. Hofstetter, Structural and spectroscopic properties of AlN layers grown by MOVPE, J. Cryst. Growth 298 (2007) 383–386.
[4] S.B. Thapa, J. Hertkorn, F. Scholz, G.M. Prinz, R.A.R. Leute, M. Feneberg, K. Thonke, R. Sauer, O. Klein, J. Biskupek, U. Kaiser, Growth and studies of Si-doped AlN layers, J. Cryst. Growth 310 (2008) 4939–4941.
[5] S.B. Thapa, J. Hertkorn, F. Scholz, G.M. Prinz, M. Feneberg, M. Schirra, K. Thonke, R. Sauer, J. Biskupek, U. Kaiser, MOVPE growth of high quality AlN layers and effects of Si doping, Phys. Status Solidi C 5 (6) (2008) 1774–1776.
[6] C.F. Shih, N.C. Chen, S.Y. Lin, K.S. Liu, AlGaN films grown on (0001) sapphire by a two-step method, Appl. Phys. Lett. 86 (2005) 211103.
[7] S. Nakamura, The roles of structural imperfections in InGaN-based blue light-emitting diodes and laser diodes, Science 281 (1998) 956–961.
[8] A. Osinsky, S. Gangopadhyay, R. Gaska, B. Williams, M.A. Khan, D. Kuksenkov, H. Temkin, Low noise p-π-n GaN ultraviolet photodetectors, Appl. Phys. Lett. 71 (1997) 2334–2336.
[9] J.-S. Park, D.W. Fothergill, X. Zhang, Z.J. Reitmeier, J.F. Muth, R.F. Davis, Effect of carrier blocking layers on the emission characteristics of AlGaN-based ultraviolet light emitting diodes, Jpn. J. Appl. Phys. 44 (2005) 7254–7259.
[10] F. Habel, P. Brückner, F. Scholz, Marker layers for the development of a multistep GaN FACELO process, J. Cryst. Growth 272 (2004) 515–519.
[11] K. Hiramatsu, K. Nishiyama, M. Onishi, H. Mizutani, M. Narukawa, A. Motogaito, H. Miyake, Y. Iyechika, T. Maeda, Fabrication and characterization of low defect density GaN using facet-controlled epitaxial lateral overgrowth (FACELO), J. Cryst. Growth 221 (2000) 316–326.
[12] R. Matsuoka, T. Okimoto, K. Nishino, Y. Naoi, S. Sakai, AlGaN epitaxial lateral overgrowth on Ti-evaporated GaN/sapphire substrate, J. Cryst. Growth 311 (2009) 2847–2849.
[13] S. Mochizuki, T. Detchprohm, S. Sano, T. Nakamura, H. Amano, I. Akasaki, Reduction of threading dislocation density in $Al_xGa_{1-x}N$ grown on periodically grooved substrates, J. Cryst. Growth 237-239 (Part 2) (2002) 1065–1069.
[14] K. Engl, M. Beer, N. Gmeinwieser, U.T. Schwarz, J. Zweck, W. Wegscheider, S. Miller, A. Miler, H.J. Lugauer, G. Brüderl, A. Lell, V. Härle, Influence of an in situ-deposited SiN_x intermediate layer inside GaN and AlGaN layers on SiC substrates, J. Cryst. Growth 289 (2006) 6–13.
[15] S. Tanaka, M. Takeuchi, Y. Aoyagi, Anti-surfactant in III-nitride epitaxy-quantum dot formation and dislocation termination, Jpn. J. Appl. Phys. 39 (2000) 831–834.
[16] O. Klein, J. Biskupek, U. Kaiser, K. Forghani, S.B. Thapa, F. Scholz, Simulation supported analysis of the effect of SiN_x interlayers in AlGaN on the dislocation density reduction, J. Phys.: Conf. Ser. 209 (2010) 012018.
[17] K.J. Lee, E.H. Shin, K.Y. Lim, Reduction of dislocations in GaN epilayers grown on Si(1 1 1) substrate using Si_xN_y inserting layer, Appl. Phys. Lett 85 (2004) 1502–1504.
[18] O. Contreras, F.A. Ponce, J. Christen, A. Dadgar, A. Krost, Dislocation annihilation by silicon delta-doping in GaN epitaxy on Si, Appl. Phys. Lett. 81 (25) (2002) 4712–4714.
[19] J. Hertkorn, P. Brückner, S.B. Thapa, T. Wunderer, F. Scholz, M. Feneberg, K. Thonke, R. Sauer, M. Beer, J. Zweck, Optimization of nucleation and buffer layer growth for improved GaN quality, J. Cryst. Growth 308 (2007) 30–36.
[20] J. Hertkorn, F. Lipski, P. Brückner, T. Wunderer, S.B. Thapa, F. Scholz, A. Chuvilin, U. Kaiser, M. Beer, J. Zweck, Process optimization for the effective reduction of threading dislocations in MOVPE grown GaN using in situ deposited SiN_x masks, J. Cryst. Growth 310 (2008) 4867–4870.
[21] K. Forghani, M. Gharavipour, M. Klein, F. Scholz, O. Klein, U. Kaiser, M. Feneberg, B. Neuschl, K. Thonke, In-situ deposited SiN_x nanomask for crystal quality improvement in AlGaN, Phys. Status Solidi (c), in press.
[22] G. Radnoczi, A. Barna, Transmission electron microscopy characterization of hard coatings and films: sample preparation aspects and results, Surf. Coat. Technol. 80 (1996) 89–95.
[23] P.B. Hirsch, A. Howie, R. Nicholson, D.W. Pashley, M.J. Whelan, Electron Microscopy of Thin Crystals, Butterworths, London, 1965.
[24] E. Van Cappellen, J.C. Doukhan, Quantitative transmission X-ray microanalysis of ionic compounds, Ultramicroscopy 53 (1994) 343–349.
[25] M.J. Hÿtch, E. Snoeck, R. Kilaas, Quantitative measurement of displacement and strain fields from HREM micrographs, Ultramicroscopy 74 (1998) 131–146.
[26] J.P. Hirth, J. Lothe, Theory of Dislocations, Wiley, New York, 1982.
[27] H. Lahrèche, P. Vennéguès, B. Beaumont, P. Gibart, Growth of high-quality GaN by low-pressure metal-organic vapour phase epitaxy (LP-MOVPE) from 3D islands and lateral overgrowth, J. Cryst. Growth 205 (1999) 245–252.
[28] M.J. Kappers, R. Datta, R.A. Oliver, F.D.G. Rayment, M.E. Vickers, C.J. Humphreys, Threading dislocation reduction in (0001) GaN thin films using SiN_x interlayers, J. Cryst. Growth 300 (2007) 70–74.
[29] K. Forghani, M. Klein, F. Lipski, S. Schwaiger, J. Hertkorn, R.A.R. Leute, F. Scholz, M. Feneberg, B. Neuschl, K. Thonke, O. Klein, U. Kaiser, R. Gutt, T. Passow, High quality AlGaN epilayers grown on sapphire using SiN_x interlayers, J. Cryst. Growth 315 (2011) 216–219.
[30] Y. Kato, S. Kitamura, K. Hiramatsu, N. Sawaki, Selective growth of wurtzite GaN and $Al_xGa_{1-x}N$ on GaN/sapphire substrates by metalorganic vapor phase epitaxy, J. Cryst. Growth 144 (1994) 133–140.
[31] B. Neuschl, K.J. Fujan, M. Feneberg, I. Tischer, K. Thonke, K. Forghani, M. Klein, F. Scholz, CL and PL study on AlGaN layers grown with SiN_x interlayers, Appl. Phys. Lett. 97 (2010) 192108.
[32] H.K. Cho, J.Y. Lee, K.S. Kim, G.M. Yang, J.H. Song, P.W. Yu, Effect of buffer layers and stacking faults on the reduction of threading dislocation density in GaN overlayers grown by metalorganic chemical vapor deposition, J. Appl. Phys. 89 (2001) 2617–2621.
[33] D.N. Zakharov, Z. Liliental-Weber, B. Wagner, Z.J. Reitmeier, E.A. Preble, R.F. Davis, Structural TEM study of nonpolar a-plane gallium nitride grown on (11-20) 4H-SiC by organometallic vapor phase epitaxy, Phys. Rev. B 71 (2005) 235334.
[34] M. Hao, S. Mahanty, T. Sugahara, Y. Morishima, H. Takenaka, J. Wang, S. Tottori, K. Nishino, Y. Naoi, S. Sakai, Configuration of dislocations in lateral overgrowth GaN films, J. Appl. Phys. 85 (1999) 6497–6501.
[35] C. Stampfl, C.G. Van de Walle, Energetics and electronic structure of stacking faults in AlN, GaN, and InN, Phys. Rev. B 57 (1998) 052–055.

Please cite this article as: O. Klein, et al., J. Crystal Growth (2011), doi:10.1016/j.jcrysgro.2011.03.050